Solar Energy 301 (2025) 113934

Contents lists available at ScienceDirect

Solar Energy

journal homepage: www.elsevier.com/locate/solener

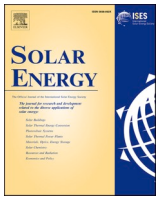

Analysis of light collection in GaAs/Si HJT four-terminal solar cell system based on spectral splitting and polymeric wedged optics: a role for diffusive lateral supports

Mehdi Ahmadi [a,b], Roberto Pagano [a,*], Fabio Matera [a], Matteo Bonomo [c,f,*], Simone Galliano [c], Iacopo Benesperi [c], Claudia Barolo [c,g], Daniela Fontani [d], Floriana Morabito [e], Andrea Farina [e], Silvia Maria Pietralunga [e,*], Salvatore Antonino Lombardo [a]

[a] CNR Institute for Microelectronics and Microsystems, VIII Strada 5, Catania 95123, Italy
[b] University of Catania, Department of Physics and Astronomy, Via Santa Sofia, 64, Catania 95123, Italy
[c] University of Turin, Department of Chemistry, NIS Interdepartmental Centre, INSTM Reference Centre and ICxT Interdepartmental Centre, Via Quarello 15/A, Torino, TO 10135, Italy
[d] CNR – National Institute of Optics-Largo Fermi 6, Florence 50125, Italy
[e] CNR Institute for Photonics and Nanotechnologies, piazza Leonardo da Vinci 32, Milan 20133, Italy
[f] Department of Basic and Applied Science for Engineering, La Sapienza University of Rome, Via del Castro Laurenziano 7, Rome 00161, Italy
[g] Institute of Science, Technology and Sustainability for Ceramics (ISSMC-CNR), Via Granarolo 64, Faenza 48018, Italy

ARTICLE INFO

Keywords:
GaAs/Si HJT four-terminal solar cells
Spectral splitting
Polymeric wedged prism
Low-gain non-imaging asymmetric optical concentrator
Indoor and outdoor photovoltaic solar system characterization

ABSTRACT

In this work a system combining a GaAs and Si heterojunction cells with optical components in a four-terminal solar cell configuration is presented. This system achieves optical low gain non-imaging asymmetric concentration and spectral splitting in order to enhance energy conversion specific to each cell, and represents a promising pathway to overcome the limitations and improve the efficiency of conventional photovoltaic systems. The split of the solar spectrum is realized by integrating into the system a specifically designed polymeric dielectric prism with light waveguide capability and high transmittance, coupled with a tailored dichroic mirror that reflects wavelengths shorter than 805 nm and transmits longer ones. In view of optimizing its performance, we critically investigate the optical performance of each component and of the system as a whole, at different light source incident angles and different colors of the side covers in a controlled indoor test environment. Moreover, outdoor tests at four fixed system orientation angles and for different side color cover cases have been performed. 4T system efficiency is studied both in indoor with a solar simulator and in outdoor under natural sunlight. The experimental results provide some clear indications to improve the system's performance, highlighting the importance of the incident angle of the source and of color of the covers to boost light collection.

1. Introduction

The global demand for sustainable energy solutions is accelerating due to increasing energy consumption and the urgent need to mitigate climate change. Among renewable energy sources, photovoltaic (PV) technology is at the forefront of efforts to reduce greenhouse gas emissions. However, conventional single-junction solar cells are fundamentally constrained by the Shockley–Queisser efficiency limit, which has motivated extensive research into advanced PV architectures capable of overcoming these intrinsic limitations [1–4]. Multi-junction solar technology is currently the most popular way to overcome these efficiency limitations [5–7]. Photovoltaic cells made with multiple layers of semiconductor material can have different band gaps and absorb a broader range of wavelengths. By capturing and converting

* Corresponding authors at: CNR Institute for Microelectronics and Microsystems, Ottava Strada, 5, Catania 95121, Italy (R. Pagano); University of Turin, Department of Chemistry, NIS Interdepartmental Centre, INSTM Reference Centre and ICxT Interdepartmental Centre, Via Quarello 15/A, Torino, TO 10135, Italy (M. Bonomo); CNR Institute for Photonics and Nanotechnologies, Piazza Leonardo da Vinci, 32, Milan 20133, Italy (S.M Pietralunga).
E-mail addresses: roberto.pagano@cnr.it (R. Pagano), matteo.bonomo@unito.it (M. Bonomo), silviamaria.pietralunga@cnr.it (S.M. Pietralunga).

https://doi.org/10.1016/j.solener.2025.113934
Received 29 May 2025; Received in revised form 15 August 2025; Accepted 25 August 2025
Available online 12 September 2025

some energy that would otherwise be lost, multijunction solar cells can improve the energy conversion efficiency of a conventional single-junction PV cell. However, while multi-junction solar cells offer high efficiency, they have practical limitations, including manufacturing complexity, high cost, fragility, and maintenance. [8,9]. On the other hand, the spectral splitting technique may provide an innovative and promising alternative to conventional multi-junction cells [10,11]. By combining the low-cost advantage of silicon heterojunction (Si HJT) solar cells and the high efficiency of gallium arsenide (GaAs) cells, coupled with "ad hoc" optics that guide and split sunlight wavelength components, the GaAs/Si HJT four-terminal (4T) solar cell system emerges as a promising alternative. This smart "low-cost" technological approach leverages spectral splitting techniques to optimize energy conversion by directing different portions of the solar spectrum to semiconductor materials that are best suited to absorb them efficiently [12–16].

In a previous study, a 4T PV system was developed using two coupled mini-modules [12,14,15]. One module comprised three Si SHJ cells connected in series and another composed of two GaAs cells in series. The optical matching between these sub-modules was achieved using two identical dichroic mirrors (DM) placed at a 45° incidence angle on both sides. The dichroic filter cutoff was set at 805 nm, meaning that wavelengths shorter than 805 nm were reflected toward the GaAs cells, while longer wavelengths were transmitted to the underlying Si SHJ cells. The Si HJT module was bifacial, allowing it to collect not only the transmitted light but also the albedo radiation from the surroundings, enhancing its overall performance. In this scenario, advanced light management strategies are essential to further enhance the performance of the proposed system. Recent innovations such as polarization-independent beam splitting and the incorporation of nanostructured materials like aluminum nanoparticles for improved light trapping in thin-film solar cells demonstrate significant potential for increasing the effective optical path and enhancing photon absorption [16–22]. Moreover, the bifacial configuration of the Si HJT cell enables the harvesting of diffused light, a feature that is particularly beneficial under outdoor conditions. Field studies have shown that parameters such as albedo, tilt, and azimuth angles play a pivotal role in determining the energy yield of bifacial PV modules [23–26]. Another theoretical study proposed an advanced spectral splitting approach and light management that combines a dichroic mirror with a light-guiding wedge dielectric prism (WDP). This design was expected to enhance the collection of randomly oriented diffused light by directing the visible (VIS) spectrum toward the GaAs cells through reflection, thereby improving optical efficiency [27].

Building on these concepts, our work focuses on the practical realization, testing, and optimization of a 4T PV system featuring a bifacial Si HJT cell and a monofacial GaAs cell, optically coupled using a dichroic mirror and a custom-designed polymeric dielectric wedge prism, like the design proposed in [27]. The use of a polymeric material instead of glass for the dielectric wedge in photovoltaic applications can offer several advantages, particularly when waveguiding properties are required. Polymeric materials can be easily engineered to possess precise optical characteristics, which is essential for efficient light trapping and guiding: for example, their chemical composition could be tuned to tailor the dielectric constant and minimizing absorption losses in the relevant spectral range. Additionally, polymers are generally lighter, allowing for easier integration into complex module architectures and potentially enabling cost-effective, large-scale manufacturing. Being in a 4T PV design the cells not directly stacked, as in the multi-junction PV technology, and not connected in series, the electrical matching is not the major issue, as also in [13,14]. Rather, the primary challenge is to design and build an effective optical coupling. On the one hand, the spectral splitting coupled with the "waveguide" approach allows to solve the problem of needing semi-transparent top PV modules, as in conventional multijunction PV cell; on the other hand, however, it requires to have a very efficient light management. Therefore, in this work we prioritize to the study of the optical coupling, which yet require to be optimized, and we decided to simplify the experimental set-up by working with individual cells rather than full modules. This eliminates the necessity of electrically matching the two sub-cells, allowing us to focus, isolate, and analyze the optical effects with high precision. Furthermore, by considering a previous study that showed how effective the color of the background would be on the 4T PV system [12], our study incorporates an investigation into the impact of different colors of the external cladding surface of the system on its performance. We evaluate the effect of white versus black covers over the overall efficiency. White covers are expected to enhance the system's collection of the diffused and albedo-reflected component of sunlight, thereby allowing to exploit not only the bifacial characteristic of the Si HJT cell, but also and ultimately improving the overall performance of the 4T PV system. In contrast, black covers, which have higher absorption, are expected to minimize the collection of these additional light sources, thus reducing the light collection and efficiency of the 4T PV system. To quantitatively assess the performance of our system, we separately measured the short-circuit current (I_{SC}) of the GaAs and Si HJT cells under different configurations. This enabled a precise evaluation of the overall optical coupling efficiency of the 4T system, providing valuable insights into its spectral light management capabilities.

2. Experimental

The four-terminal system discussed in this work consists of two solar cells whose current–voltage (I-V) and photocurrent characteristics are separately measured. Such approach allows to focus on the system's optical efficiency, which is the major issue to investigate for evaluating the advantages given by the present approach based on non-imaging concentration through a dielectric wedge. The electrical optimization, in particular the optimization of the series resistance and of the fill factor (i.e. the ratio between the maximum power and the ideal theoretical power of the system), is a minor aspect, that can be simply solved once the proper optical concentration conditions are found, and it is not addressed in this paper. As solar cells we have used a commercial GaAs cell from Rera Solutions [29] [with an active area of 2.0×2.0 cm^2, and a bifacial Si HJT made by 3SUN in a M2 pseudo-square format [30], with $V_{OC} = 730$ mV, $J_{SC} = 38$ mA/cm^2, bifaciality factor = 90 %, and power conversion efficiency (PCE) of 22–23 % under standard test conditions (STC). In the case of the GaAs cell a gap of approximately 0.5 cm between the glass surface of the module and the cell itself is present, and this introduce an air gap [20]. This gap can reduce the system performance as discussed later. The Si cell has been manually cut into 2.3×3.8 cm^2 and contacted through copper ribbons coupled to the cell by using an electrically conductive adhesive (ECA) glue. The solar cells were then coupled to a $2.5 \times 3.6 \times 0.1$ cm^3 dichroic mirror (DM) from Thorlabs [31], and to a custom-made wedged dielectric prism (WDP) having $2.0 \times 3.1 \times 3.7$ cm^3 triangular cross-section area. Fig. 1a) shows a schematic image of the exact position of each element. The GaAs and Si HJT cells are in contact with the surfaces of the WDP containing the minor leg and the hypotenuse, respectively. To be precise, the DM is sandwiched between the WDP surface and the Si HJT cell.

The WDP used in the experiment, shown in Fig. 1b), is made of a thermosetting polyurethane resin, shaped as a wedge by using a mold technique. A 1:1 mixture of polyol blend and the isocyanate prepolymer (XP541 and XH181, respectively) developed in collaboration with Demak Polymers s.r.l., was selected due to its high transmittance and excellent resilience to both thermal and radiative stress [32]. Moreover, it stands out thanks to a refractive index as high as 1.503, very similar to that of the glass (for more details on the fabrication of the WDP, please, refers to the Supporting Information file).

The overall system of solar cells, DM, and WDP, as shown in Fig. 1a, is held together thanks to a spine, composed of two lateral pieces and a rear one, having a thickness of 9 mm, 3D-printed from a white polylactic acid (PLA) filament using a Makerbot Replicator 2 printer. The

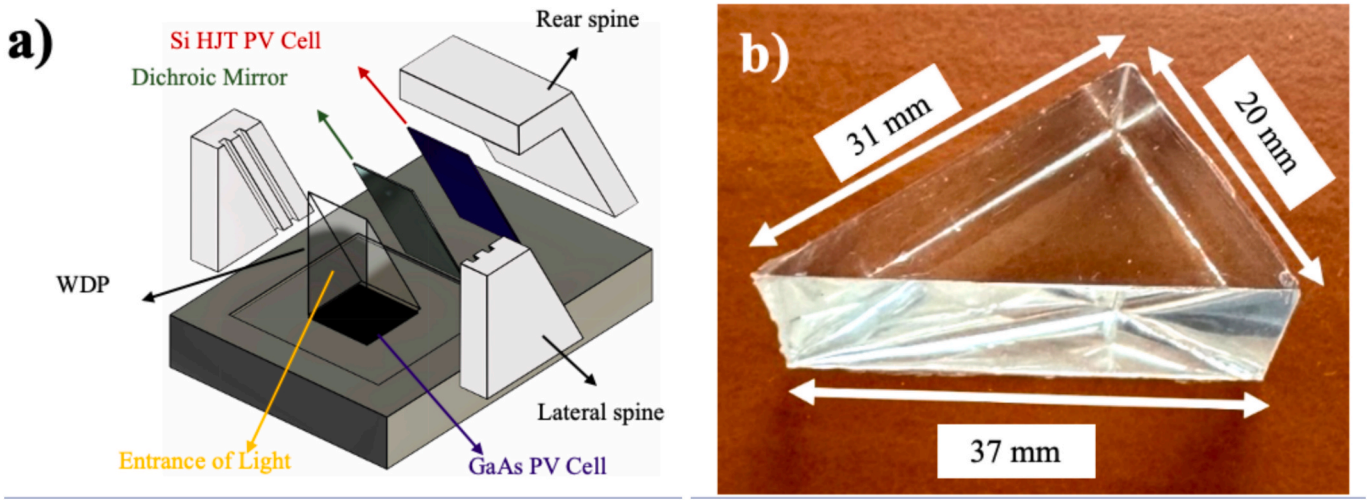

Fig. 1. A) Schematic of the 4T system setup consisting of a GaAs and a Si HJT cell, the dichroic mirror, the custom-made wedged dielectric prism, the spine; b) Image of the custom-made polymeric wedged dielectric prism used in the experiment.

temperature of the printer's nozzle was set at 210 °C to print 0.3 mm layers at 50 mm/s and 100 % infill with the help of Makerbot's slicing software. The spine pieces were designed with PTC Onshape. They were covered on the outside with a coloured cover. The only directly exposed light ingress of the 4T PV system was the surface of WDP, specifically the one containing the longest perpendicular side.

To characterize the system's optical components, we measured the transmittance (T) and reflectance (R) of the DM and of the WDP for $\alpha = 45°$ and $\alpha = 90°$, respectively, (from the longer cathetus where the light enter) and the external quantum efficiency of both cells in the 300 nm to 1100 nm range with a Bentham PVE300 system, an all-in-one system, including a broad-wavelength light source, a monochromator, an integrating sphere and calibrated photodiodes, which allows to perform easily reflectance, transmittance and quantum efficiency measurement. Moreover, using the same instrumentation R and T were also measured for the 3D printed spines, normally oriented with respect to the light source, covered in white, in black, and with no cover.

In this work, two types of experiments were performed on the whole 4T PV system: in one case, the spine is covered with a white tape (3 M Scotch 101E), henceforth referred to as the "white" covered spines case, while in the second case they were covered with a black fabric, referred to as "black" covered spines.

The WDP in conjunction with the DM works as a lightguide, wavelength splitter and low gain asymmetric optical non-imaging concentrator, meaning that only the VIS light impinging onto the smallest WDP face is concentrated [27]. When light enters into the system, it is separated into its near infra-red (NIR) and visible (VIS) portions, and guided internally to the PV cells [27]. In this work the VIS and NIR components of the light spectrum is considered be between 300 nm and 805 nm and between 805 nm to 1100 nm, respectively. Since the DM was designed for reflecting and transmitting wavelengths shorter and longer than 805 nm, respectively, [14], when the light is incident to its surface, the NIR portion is transmitted to the Si cell, while the VIS portion is reflected into the WDP. The VIS light, due to the total internal reflection at the WDP sides, will eventually reach the GaAs PV cell. This spectral splitting process, therefore, helps to decrease the overall optical impinging power and therefore the temperature of the cells, and consequently it increases the overall efficiency of the PV system [18].

The performance of the 4T system was tested indoor and outdoor. Moreover, the system was tested, as previously discussed, using two different covers on the spines: black and white. With the black cover, the system is entirely dependent on solar light entering through the exposed surface of the WDP. Instead, by using white covered spines not only the direct but also some diffused and albedo reflected light play an important role in the energy harvesting and conversion process, as described below.

The sketch shown in Fig. 2a) illustrates the system under the sunlight exposure. The system is south-facing and four important angles are identified: α, which is the angle between the incident light and the normal to the exposed WDP surface; β, which is the angle between the input surface of the WDP and the horizontal; θ, which is the sun elevation measured from the horizon of the site, and γ, which is the solar azimuth angle. It should be noted that in the indoor measurements, where a solar simulator is used, θ is always 90°, and α is equal to β.

In the indoor experiments, the system was oriented in order to have the α angle varying from 10° to 60° in a step of 5°. The incident angle in outdoor measurements is calculated by Eq. (1), as follows:

$$\alpha = \arccos(-\sin(\beta) \bullet \cos(\gamma) \bullet \cos(\theta) + \cos(\beta) \bullet sin\beta(\theta)) \quad (1)$$

It should be noted that outdoor the incidence angle α changes throughout the day. Therefore, in outdoor tests, the 4T system was positioned facing to the south, so that, at noon, when the sun elevation was maximum, in accordance to the time value registered by the nearby meteorological station, the α angle, α_{noon}, was 10°, 20°, 30° and 40°. In this way, its performances at noon, are comparable with those obtained indoor. The beta angle was derived accordingly to Eq. (1) by considering the position of the sun on that particular day, while γ at noon was close to 180° for all test. The experimental conditions in the outdoors are summarized in Table 1.

For the indoor experimental characterization of the 4T system, an ABET TECHNOLOGIES – Sun 3000, solar simulator having AAA Class was used, with standard AM1.5G spectrum. In this case, to measure the incident power at each angle, a silicon-calibrated cell was used as reference, oriented at the same angle α and height as the 4T PV system. The 4T PV system was tested at an ambient temperature set to 20 °C with the aid of a fan ventilation on the 4T PV system. As the Si PV cell was cut mechanically, the V_{OC} decreased, and the series resistance increased due to the non-fully optimized series connection by ribbons [14]. Considering these reasons, an I-V characterization of the silicon solar cell in optimal conditions was not possible. Therefore, only the short circuit current (I_{SC}) was measured at each angle, after ensuring that its values were not influenced by the large series resistance of the cell itself. All indoor measurements were performed using a Keithley 4200 source measure unit (SMU) parameter analyzer, in the voltage range from −0.5 V to + 1.1 V.

Outdoor tests were carried out in Catania, Italy (37°26′ N, 15°4′ E) from 9:30 a.m. to 4p.m. The PV cell currents were evaluated by the

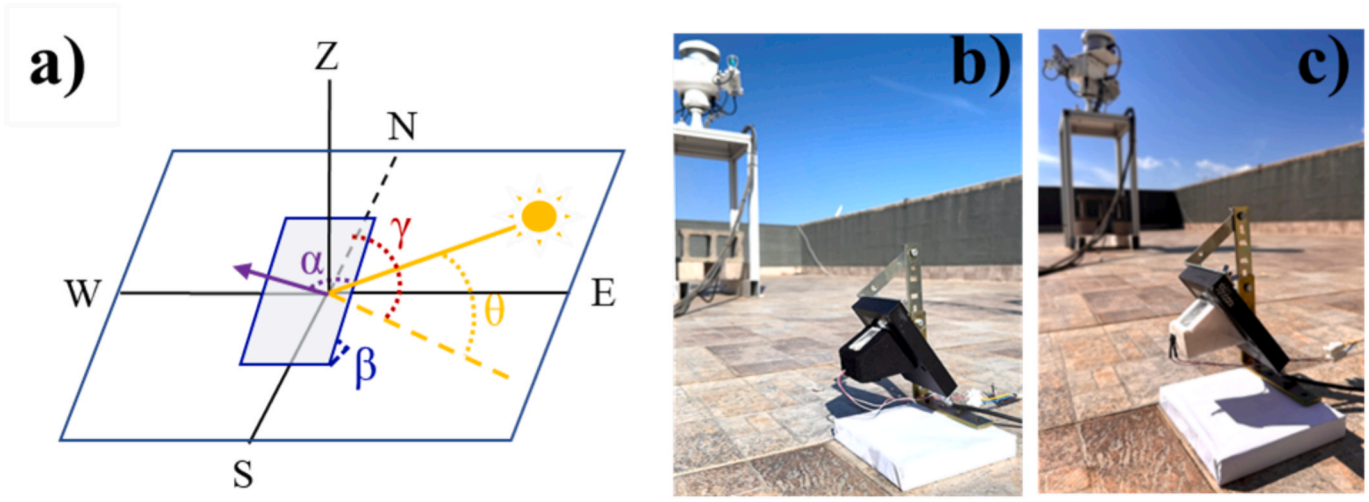

Fig. 2. a) Sketch of the surface of the 4T system highlighting the four characteristic angles α, β, γ, and θ. b) and c) Images of the 4T system during outdoor measurements with a black and a white cover, respectively.

Table 1
Summary of the outdoor experiments including the name of the experiment, the date, the most significant angles and the colour of the cover used. *Noon time is in accordance with the nearby meteorological station.

File Name	Date (dd/mm/yyyy)	Noon Time* (hh:mm)	α_{noon} (degree)	θ_{noon} (degree)	β (degree)	Color of cover
W-10	01/10/2024	11:43	10	38	42	White
W-20	16/10/2024	12:45	20	43	27	White
W-30	04/12/2024	11:50	30	30	30	White
W-40	30/10/2024	11:43	40	38	12	White
B-10	11/12/2024	11:53	10	29	51	Black
B-20	16/12/2024	11:55	20	29	41	Black
B-30	06/12/2024	11:50	30	30	30	Black
B-40	09/12/2024	11:52	40	29	21	Black

voltage drop across resistors connected in series to the cells, of 1.2 Ω and 1.15 Ω for the GaAs and the Si HJT PV cell, respectively, and recorded by a Campbell CR1000 data logger.

An EKO STR-22G Sun Tracker, an EKO MS-57 Pyrheliometer, and two MS-711 EKO Spectroradiometers were used for the spectral monitoring of the direct, the diffused, and of the global solar radiation, respectively. Two MS-80 EKO pyranometers mounted back-to-back and tilted at the same angle of the 4T system, were used to measure the intensity of the horizontal solar radiation providing in real-time albedo and solar irradiance. All data related to the solar spectrum and ambient light were acquired in the wavelength range from 300 nm to 1100 nm throughout the day. Ambient temperature, humidity, and solar noon time were collected from the nearby weather station [34].

3. Results and discussion

The transmittance and reflectance of the DM and of the WDP, and the quantum efficiency of the Si-HJT and GaAs PV cells are shown in Fig. 3a). WDP transmittance up to 370 nm is almost null in agreement to what reported for 1 cm polymeric film (see additional Supporting Data). Still, after that, it sharply increased to almost 93 % across the entire wavelength range from 400 nm to 1100 nm. In reflection measurement, the WDP shows a low (≈6%) and stable reflectance across the entire wavelength range. The DM transmittance is almost null below 805 nm and close to 98 % above, as expected at an incidence angle of 45°.

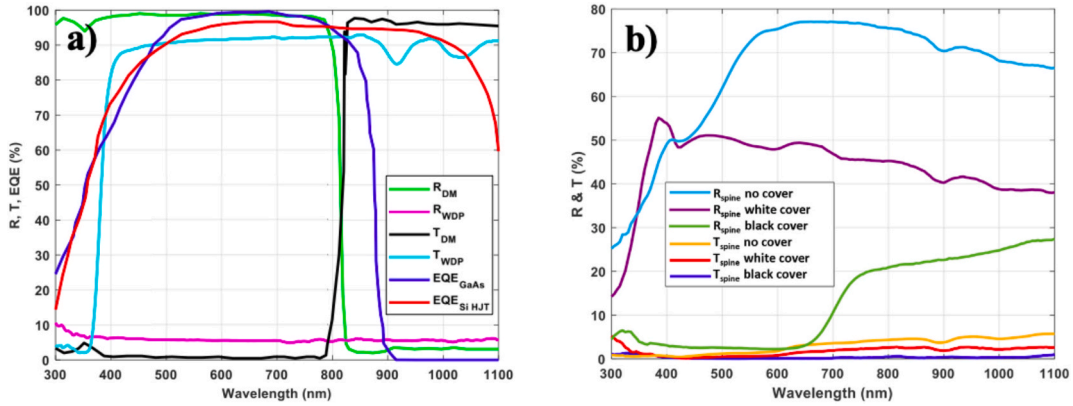

Fig. 3. A) Transmittance and reflectance of the optical components of the 4T system and the external quantum efficiency of both PV cells; b) Transmittance and reflectance of the 3D printed white lateral spines with white, black, and no covers.

Transmission below 370 nm is prevented by the absorption due to UV-stabilizers within the polymeric matrix mandatory to prevent the degradation (e.g. yellowing) of the polymer as proved in [35]. It was also verified that the variation of the cut-off wavelength and the transmittance of the DM are not appreciably altered either for an incidence angle of 0°(data not shown). The cut-off wavelength for a 0° incident angle is about 875 nm, just 70 nm shifted in the NIR region with respect to the intended cut-off wavelength at 45°. The transmittance is almost the same in value. A similar behaviour is expected for an incident angle of 90°, but in such a case with a shift of the cut-off wavelength in the direction of the blue region [36]. The GaAs PV cell demonstrates a high EQE on a wide range of wavelengths, starting from around 300 nm and extending up to approximately 900 nm beyond which it collapses. It is noted that the cut-off length of the DM (805 nm) specifically chosen for this reason, is very close to the collapse wavelength of the GaAs EQE. Assuming a reasonable shift of the cut-off wavelength of approximatively 70 nm both on the left and on the right with respect to 805 nm, as the incident angle will change for the range of planned experimental tilt angle of the system, considering the EQE of the GaAs and of the Si PV so far discussed, the effect on the cell photocurrent is expected to be mild.

Fig. 3b) reports reflectivity (R) and transmissivity (T) of the 3D printed white lateral spines with white, black, and without any covers normally oriented with respect to the light source, measured through the integrating sphere method. Note that here the measured R and T values include also the fraction of diffused light coming out from the sample. In Fig. 3b) it is evident that the reflectivity of the white spine is quite large, while the transmissivities of the black and white covered spines are, respectively almost zero and ≈3% in the red/near IR range, respectively. The transmissivity of the white covered spines, though it is only ≈3% in the red/near IR range, plays an important role in the overall system optical efficiency. This is quite evident when we compare the optical efficiencies of the systems with black and white covered spines, as we describe in detail in the following sections.

3.1. Indoor measurements

A simple Figure of Merit (FOM) derived from experimental measurements was chosen as parameter to quantitatively evaluate and compare how different conditions, such as illumination and the color of the external cover, influence the throughput of the 4T system. The FOM is defined as follows:

$$FOM = I_{SC}^{GaAs} \bullet V_G^{GaAs} + I_{SC}^{Si} \bullet V_G^{Si} \tag{2}$$

where I_{SC} is the short circuit current of the PV cell and V_G the band gap voltage of the semiconductor having value equal to 1.14 V and 1.42 V, for Si and GaAs, respectively. Fig. 4 shows the FOM as a function of the angle α for the white and black cover case. Both curves exhibit a general decreasing trend as the incident angle α increases from 10° to 60°, following a cosine law, as expected since the incident flux of light decreases as the incident angle α increases. Overall, the system works better at lower incident angles. It can be noticed that higher FOM values are found across the entire range of incident angles when the white cover is used.

To evaluate the overall efficiency of the 4T system, the ideal calculated I_{SC} of both PV cells are compared to the measured ones. The ideal I_{SC} values are evaluated by the following equations:

$$I_{Si}^{Ideal}(\alpha) = e \bullet S_{WDP} \bullet \int_{300nm}^{1100nm} (AM1,5^{*}(\lambda) \bullet T(\lambda) \bullet EQE_{Si}(\lambda))d\lambda \bullet \frac{P_{Incident(\alpha)}}{1000W/m^2} \tag{3}$$

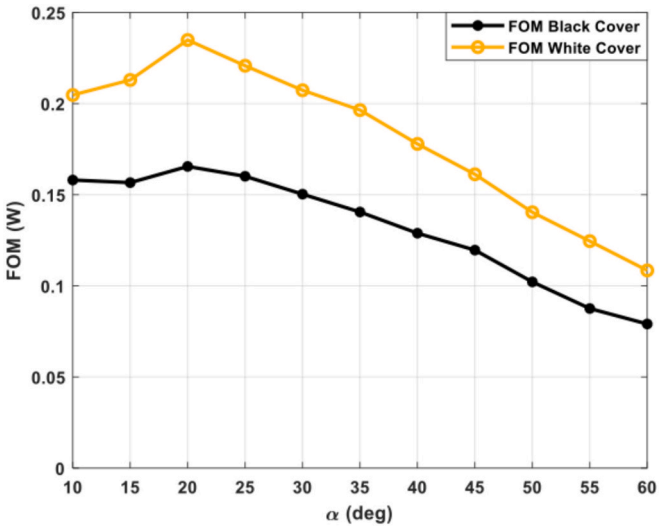

Fig. 4. The FOM defined in Eq. (2) for α angles ranging from 10° to 60° of the 4T system with the white or the black cover measured indoor.

$$I_{GaAs}^{Ideal}(\alpha) = e \bullet S_{WDP} \bullet \int_{300nm}^{1100nm} (AM1,5^{*}(\lambda) \bullet R(\lambda) \bullet EQE_{GaAs}(\lambda))d\lambda \bullet \frac{P_{Incident(\alpha)}}{1000W/m^2} \tag{4}$$

where e is the elementary charge, S_{WDP} is the WDP surface area exposed to light, AM1.5G is the global solar spectrum for air mass 1.5 at 1 sun [33], R, T, EQE_{Si} and EQE_{GaAs} are the DM reflectivity and transmittance, and the external quantum efficiencies of the Si and GaAs PV cells, respectively, and $P_{incident}$ is the measured incident optical power. It is important to note that this model, as discussed later, is an analytical ideal model that allows one to easily compare, with good precision, the experimental results with the expected ideal one and does not capture all the effects of the optics integrated into the system as the incidence angle varies. As an example, in Eq. (3), the small contribution of light directly reaching the cell is not considered and this may lead to a small underestimation of the current itself. A more rigorous model, considering the actual geometry of the WDG and the specific angle-dependent contribution of each wavelength component of light, requires optical ray tracing simulations, as previously done in [27]. It should also to be note that the model does not take in consideration the current generated by the back side of the bi-facial Si HJT cell, being the back side of the system covered by the spine.

The incident power $P_{incident}$ was obtained, as discussed in the experimental, from the I_{SC} of a Si reference cell measured at each α angles, as follows:

$$P_{Incident}(\alpha) = \frac{I_{SC}^{Ref}(\alpha)}{I_{SC}^{Ref}(0^{\circ})} \bullet 1000(\frac{W}{m^2}) \tag{5}$$

where the reference PV cell I_{SC} at 1 SUN and $\alpha = 0°$ is 136 mA.

In Fig. 5 the comparison among the ideal and measured I_{SC} for both the GaAs and Si HJT PV cells is shown for incident irradiation angles ranging from 10° to 60° and the two different cover colors used. As the angle of incidence increases, the effective area exposed to light decreases with the mentioned cosine law, resulting in an incident optical power and, consequently, a lower ideal I_{SC} for both PV cells. This simple explanation, in reality, does not take into account the contribution of the WDP combined with the DM and the effect that these produce on each single wavelength component of the light as its angle of incidence varies and therefore on the effective power that reaches each photovoltaic cell. In fact, the measured I_{SC} trend is somehow different: for the GaAs cell it increases from 10° to 20° and then decreases as expected, while for the

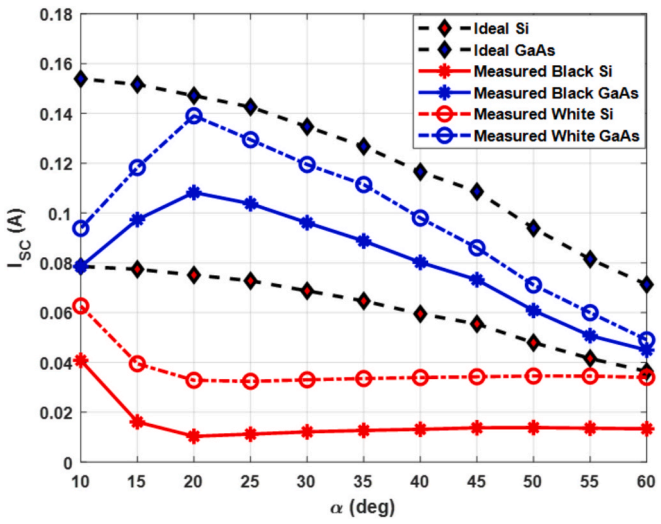

Fig. 5. Comparison of the ideal I_{SC} and the measured indoor ones for the GaAs and Si HJT PV Cells with the white or black cover for α angles ranging from 10° to 60°.

Si HJT PV cells it decreases in the range 10° to 20° and then it remains almost constant for larger α values.

The trends in Fig. 5 can be explained in terms of the role of Total Internal Reflection (TIR) at the back and bottom sides of the WDP. Actually, at odds with the situation described in [27], where optimum optical coupling is supposed between the WDP and the solar cells and TIR only occurs at the top surface of the wedge, in the present implementation air gaps are present at the bottom between the WDP and the dichroic mirror and between the mirror and the Si cell. Also, an air gap exists between the WDP and the input window of the GaAs cell packaging and about 5 mm of air gap are present inside the cell packaging. Therefore, TIR occurs at bottom and back surfaces as well. By considering a refractive index n = 1.5 for the WDP, the limit angle for TIR is θ_L = arcsin (1/1.5) = 41.81°. The drop in I_{SC} at the GaAs cell between 10° and 20° of incidence angle α at top is a consequence of that portion of VIS light that directly hits the back surface at grazing incidence exceeding θ_L and is reflected off by TIR. At increasing α values, TIR is no more effective at the back surface and $I_{SC}(\alpha)$ retrieves an ideal decrease cosine law. From ray tracing simulation using Zemax it is estimated a loss of efficiency between the ideal case with no air gap and the real case of approximately 5 % at $\alpha = 20°$ up to 25 % for α above 50°.

Regarding the decrease in I_{SC} of the Si HJT cell at the bottom, it can also be easily demonstrated geometrically that on the bottom side, light is highly reflected off for $\alpha > 10°$ and that TIR occurs at $\alpha > 20°$, leading to virtually negligible illumination of the HJT cell. This explains quantitatively the saturation in I_{SC}, with stray light accounting for a residual finite current value. A detailed geometric explanation is provided in the Supplementary Information and illustrated in Fig. A7.

Regarding the cover color, the I_{SC} are larger when the cover is white, for both PV cells. However, this increase is much more pronounced for the Si HJT cell, reaching nearly a 2.5-fold enhancement in the I_{SC} for the white cover versus black cover. These enhanced I_{SC} values are attributed primarily to an enhanced light trapping into the WDP, in the case of the white spines, which act as optical diffusers of the light incident from the top, and to a secondarily, but not negligible, contribution from the backside Si HJT PV cell.

To better explain the first effect, we believe that the source light reaching the top surface of the spine, similar to what happens in turbid materials [28], enters the spine and, after a few free paths, is scattered and diffused from the spine/WDP interface into the system. In such a case, the rule of 3 % of transmission, like in conventional optics, doesn't work, but a larger percentage of incoming light can be diffused inside the system, depending on the optical scattering coefficient of the material. This effect, can produce an increase of the I_{SC} current in magnitude comparable to the I_{SC} produced when the black cover is used and is more pronounced in the red and near infrared wavelength spectra. Nevertheless, for a more rigorous treatment of this behavior, further work is still required.

We now focus on the system efficiency, η^{EO}, here defined as the ratio between the measured and the ideal I_{SC} at different α angles:

$$\eta^{EO}(\alpha) = \frac{I_{SC}(\alpha)}{I_{SC}^{Ideal}(\alpha)} \tag{6}$$

η^{EO} compares the actual performance of the 4T system to its theoretical maximum ideal performance at different α. It helps to identify optical losses, due to imperfections either in the coupling between optical components and the PV cells or in the light trapping and transmission of the WDP.

The η^{EO} as a function of α for the black and white cover case is shown in Fig. 6. The η^{EO} reaches its maximum and minimum value of 75 % and 15 % for $\alpha = 20°$, for the GaAs and Si HJT PV cell, respectively, in the case of a black cover. At higher α values, the η^{EO} for the GaAs PV cell decreases to 63 %, while for the Si HJT PV cell increases to 38 %. It should be noted that the maximum η^{EO} for the Si HJT PV cell is 50 % at $\alpha = 10°$. When the white cover is used, even if for both cells almost the same trends are observed, a large difference of absolute values is found. For the GaAs the efficiency increases of about 10–20 %, while for the Si HJT the η^{EO} increases of a factor ≈3. As evident from the data of Figs. 5 and 6, the cover colour has a very significant impact on the I_{SC} and η^{EO} of the 4T system. As mentioned above, the effect is likely due to an enhanced light trapping effect into the WDP in the case of the white cover. In fact, in this case the spine acts as optical diffusers, introducing a portion of extra light coming from its top into the WDP from the lateral WDP/spine interface, and a smaller portion from the rear spine which is absorbed by the back of the bifacial Si HJT cell. Such extra- light entering the PV system is suppressed when black covers are used.

3.2. Outdoor measurements

The sun elevation and the incident angle α, calculated by Eq. (1), for all days of the outdoor measurements, are shown in Fig. 7a) and b), respectively, between 9:30 am and 4 pm. Outdoor measurements, as discussed in the experimental, were done only at four different α angles

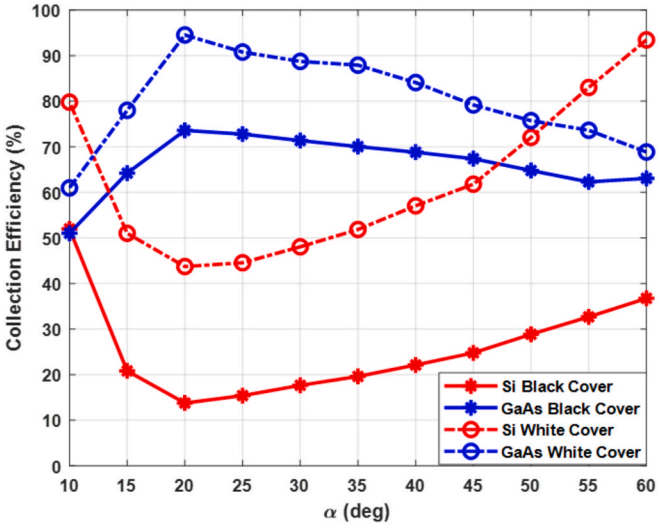

Fig. 6. Indoor electro-optical yield efficiency, η_{ν}^{EO} as defined in the text for the GaAs and Si HJT PV cell for α angles ranging from 10° to 60° and for the white and black cover cases.

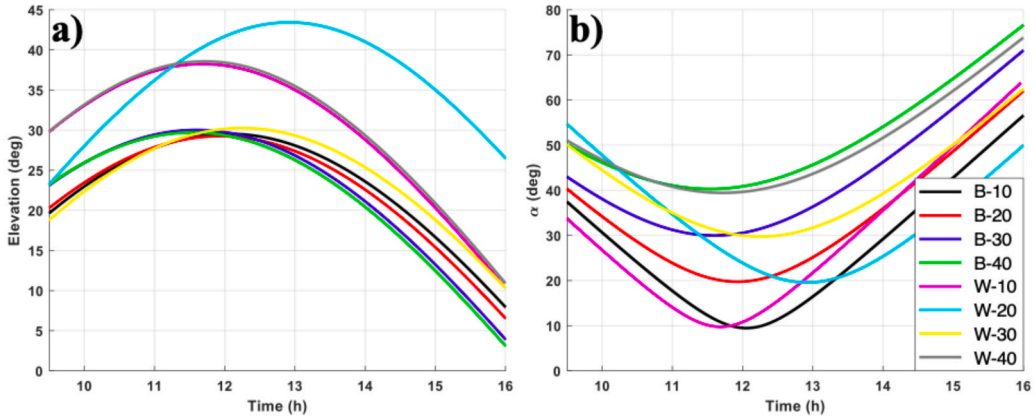

Fig. 7. A) Elevation θ and b) Incident angle α of the sun with respect to the normal of the WDP surface during the 8 days of outdoor experiments, Cyan lines, W-20, are shifted to the right because the transition from daylight saving time to solar time came into effect (Tab. 1). (For interpretation of the references to color in this figure legend, the reader is referred to the web version of this article.)

at midday (α_{noon}), i.e., ≈10°, ≈20°, ≈30°, and ≈40°, for both the white and black covers case, indicated in the legend of Fig. 7 as W-"α" and B-"α", respectively in accordance with the file name in Tab. 1. Note that in the case of the experiment relative to the white cover case $\alpha_{noon} = 20°$ (W-20), the curves, cyan lines, are shifted to the right with respect to the time axis as the transition from daylight saving time to solar time came into effect (Tab. 1).

Fig. 8 shows an example of daily variation of the direct, the corrected direct and the diffused solar flux (for the complete data set please refer to the additional Supplementary Information). These data are obtained by integrating over the 300 to 1100 nm wavelength range the spectral information measured by the spectroradiometers. The direct flux, red line in Fig. 8, which represents the solar radiation reaching the surface without being scattered or absorbed by the atmosphere, is the most intense component of the sun irradiance. The direct flux multiplied by cos(α), orange line in Fig. 8, accounts for the direct solar light flux entering into the 4T system, important to maximize the energy capture by choosing an optimized orientation of the 4T system. The diffused flux, purple lines in Fig. 8, is the part of the solar radiation that is scattered by the atmosphere. In a clear day, as considered here, its contribution is lower than that of the direct flux and less variable in time throughout the day.

Fig. 9 shows an example of the diurnal variation of the central

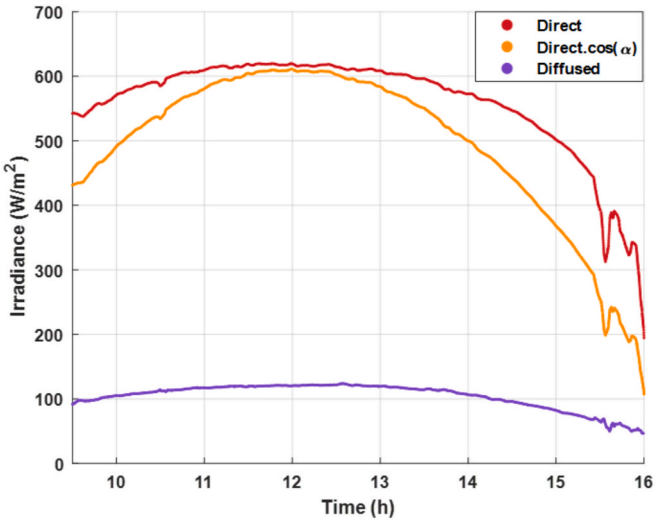

Fig. 8. Daily variation of the solar irradiance during the days for the case of $\alpha_{noon} = 10°$, $\beta = 51°$ and black cover.

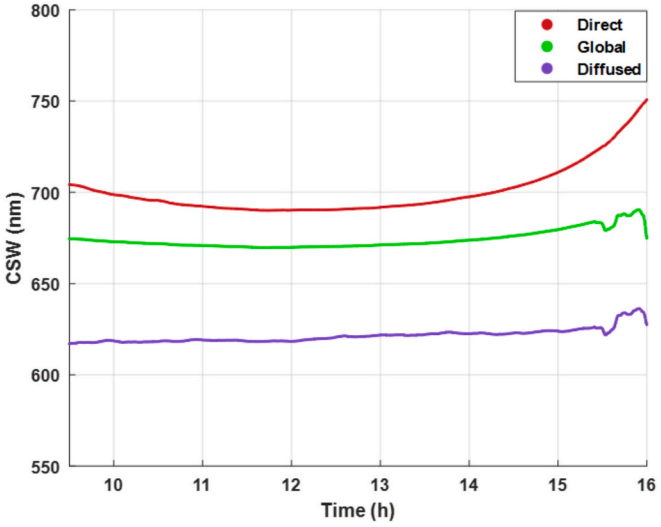

Fig. 9. Daily variation of the central spectrum wavelength for the case of $\alpha_{noon} = 10°$, $\beta = 51°$ and a black cover.

spectrum wavelength, CSW, of direct, global, and diffused solar radiation. Similar results were found for all eight days of outdoor tests. The CSW is calculated by integrating the product of wavelength and its corresponding photon flux over the entire spectrum and then normalizing by the total photon flux, as follows:

$$CSW = \frac{\int_{300}^{1100} \varnothing_S(\lambda) \bullet \lambda \bullet d\lambda}{\int_{300}^{1100} \varnothing_S(\lambda) \bullet d\lambda} \quad (7)$$

where λ is the wavelength and ϕ_S (λ) is the photon flux at wavelength λ. In fact, the solar spectrum extends from ≈300 nm to ≈3000 nm, and this is not considered by Eq. (7). The reason is that here we want to focus on the range where our solar cells show appreciable quantum efficiency.

Throughout the day, the CSW is higher for direct solar radiation, as direct sunlight is less scattered and, therefore tends to have a longer dominant wavelength. CSW is lower for the diffused light, which is subjected to scattering from the atmosphere that enhances the blue component of sunlight. The CSW of the global sunlight radiation, being a combination of the two, lies in between.

In general, we observe that in all cases the CSW shifts towards the red/IR after mid-day, an effect which is attributed to the increase of the air mass. Another aspect extremely important to underline is that the

spectrum shape shows very strong variations during the day. A tandem or multi-junction device, in which cells of different band-gap are in series, such changes would produce a noticeable fluctuation of the efficiency, because the spectrum change will be reflected in a current mismatch among the cells. On the contrary, a 4T system is very robust on this aspect, since spectrum variations would produce only very minor changes in the open circuit voltage of the matched PV modules [14].

During the outdoor tests, the angle of incidence of solar rays continuously changes, and only at noon the direct sun rays, the normal to the WDP, and the local meridian are in the same plane. Therefore, only at noon the measured I_{SC} values can be directly compared to the results of the indoor tests. Such evaluation however neglects the diffused sunlight component which for the indoor test is obviously not present. On the contrary, the ideal currents for the outdoor test have to take into account its contribution and they are calculated as it follows:

$$I_{Si}^{Ideal} = e \bullet S_{WDP} \bullet \int_{300nm}^{1100nm} (\varnothing_D(\lambda) \bullet cos(\alpha) + 0,5\varnothing_{Diff}(\lambda)) \bullet T(\lambda) \bullet EQE_{Si} \bullet d\lambda \quad (8)$$

$$I_{GaAs}^{Ideal} = e \bullet S_{WDP} \bullet \int_{300nm}^{1100nm} (\varnothing_D(\lambda) \bullet cos(\alpha) + 0,5\varnothing_{Diff}(\lambda)) \bullet R(\lambda) \bullet EQE_{GaAs} \bullet d\lambda \quad (9)$$

where ϕ_D and ϕ_{Diff} are the direct and diffused photon flux of the solar spectrum, respectively. Most of the components were already discussed for Eqs. (4) and (5) as well the limit of the model. The main difference in Eqs. (8) and (9) is that here ϕ_{Diff} is multiplied by a correction factor equal to 0.5. This constant factor considers that the diffused radiation here considered is isotropically directed over a 2π steradians solid angle and only a portion of about ½ is collected by the WDP.

Fig. 10a) and b) report the outdoor measured and ideal I_{SC} vs. time, for the case $\alpha_{noon} = 10°$, for both Si HJT and GaAs PV cells, measured in different days for the cases of the black and white cover, respectively. In general, the I_{SC} over time for all angles follows a bell-shaped curve, reaching a peak near midday when the sun is at its highest position in the sky and irradiation fluxes have the maximum intensity. Significant deviations from such trend are found when the weather is cloudy. Since such deviations are likely due to extensive solar light shielding and scattering due to the clouds, effects which are due to complex physical mechanisms and are out of the scope of the present study, we focus our analysis only to the case of the sunny periods, where the effects of the clouds are not present. In the data shown in Fig. 10a) it is possible to note a drop in the GaAs current between 10.30 h and 14 h. This drop of the current was only measured for this experimental condition. Most probably, for such condition ($\alpha_{noon} = 10°$, $\beta = 51°$, and $\theta_{noon} = 29°$), as the sun elevation is low, that is before 10:30 h and after 14 h, light reached the GaAs cell directly. Instead, between 10:30 h and 14:00 h, when the sun elevation was higher, the light reached the GaAs cell after reflecting into the dichroic mirror. In the first case the optical power reaching the GaAs cell was higher and therefore the current.

The complete set of data are included in the additional Supplementary Information, in which example of experiment performed in partly cloudy days are shown, and the effect of passing clouds is reproduced by the experimental data collected.

On the basis of the I_{SC} data of Fig. 10, Fig. 11 reports an example of the efficiency, η^{EO}, as defined in Eq. (6), as a function of the time for $\alpha_{noon} = 10°$ and for the black and white cover case, represented with continuous or dashed lines, respectively (for the complete data set please refer to the Supplementary Information). In general, the performance of the PV cells depends strongly on the system orientation, indicating that optimal angles can significantly enhance or reduce the efficiency, as also shown by the indoor results. Moreover, when the black covers are used, the GaAs cell η^{EO} in most cases outperforms the Si HJT cell. On the contrary, with the white covers, it is the Si HJT PV to show higher η^{EO} values. The other major feature to underline is that in the case of white covers, values of η^{EO} larger than 100 % for the Si HJT cell can be measured. As previously noted, we attribute the effect to an enhanced contribution of light into the WDP in the case of the white spines. These act as optical diffusers, so some of the light incident from the top on

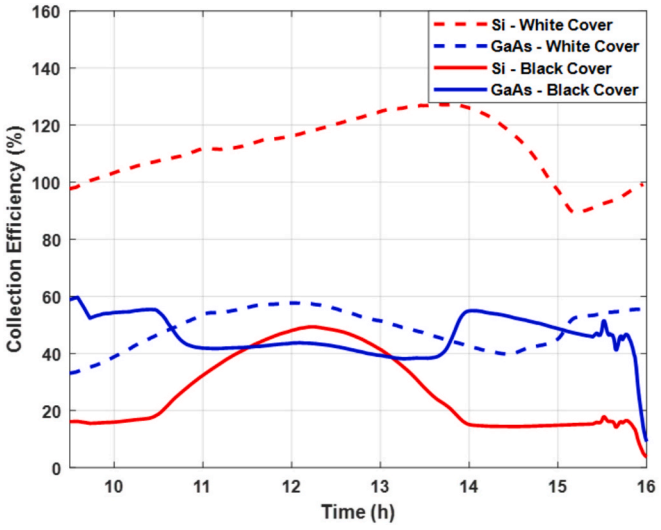

Fig. 11. Outdoor efficiency at an incident angles $\alpha_{noon} = 10°$ for the Si HJT and GaAs PV cells for the cases of the white and black side cover.

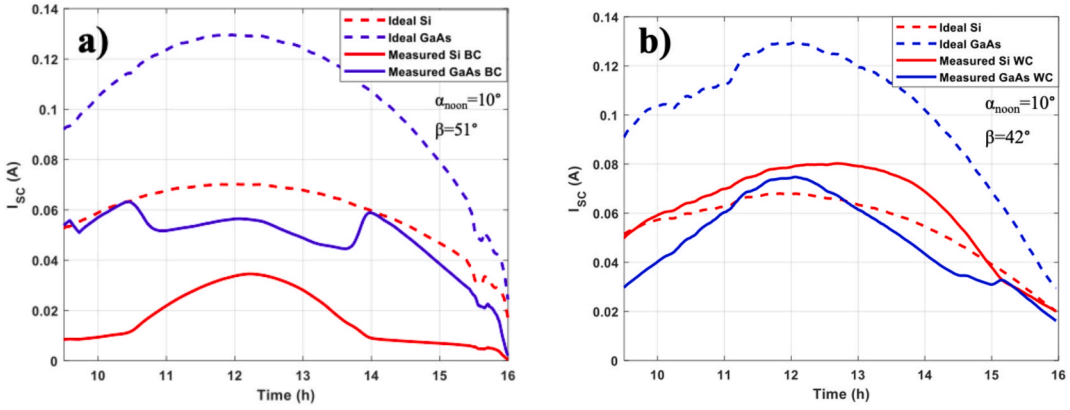

Fig. 10. Ideal and measured I_{SC} during the four days of the outdoor tests for the 4T PV system for $\alpha_{noon} = 10°$ and a) the black and b) and white cover case, respectively.

them is diffused from the lateral WDP/spine surface into the WDP. Moreover, in outdoor, since the diffused component of the sun irradiance is non negligible, as shown in Fig. 8, part of this light is transmitted laterally and from the back by spine into the PV system and collected by the solar cells. Such an explanation agrees with the observation that in the morning or in the afternoon η^{EO} increases very much, i.e., when the spines are irradiated directly by the sun at grazing angles of elevation, in the east- west direction. The explanation of the efficiency enhancement as due to light diffusion from the spines is also supported by the fact that the η^{EO} has a strong increase for the Si cell but a weak one for the GaAs cell, in agreement with transmittance data of the spine (Fig. 3b), which is almost zero in the blue-red, and about 3 % in the red-NIR. The η^{EO} values above 100 % registered outdoor are therefore explained by the fact these extra sources of light are not considered by the ideal model. This effect is dominant in the outdoor experiments, where sunlight has a non-negligible diffused component that is not present, or almost null, indoor.

Fig. 12 reports the data of η^{EO} vs. α comparing indoor and outdoor results for the black and white cover cases.

The outdoor data of η^{EO} are at noon, where a direct comparison of indoor and outdoor is possible. For the black cover case (Fig. 12 a)) the values of η^{EO} for GaAs and Si HJT cells have similar values and almost the same trend for both indoor and outdoor tests. These results of η^{EO} vs. α also show quite similar trends when compared to the theoretical evaluations reported in [27] for the case of the GaAs cell. On the contrary, the comparison between the theoretical result and the expected one for the case of Si cells is not entirely consistent and the explanation is currently under study. However, when we consider the case of the white covers (Fig. 12b)), major changes are observed for the case of the Si cell, where a large yield enhancement is found, which in the outdoor case leads even to $\eta^{EO} > 100$ %. As explained before, the effect can be attributed to additional diffusion of light into the WDP in the case of the white cover, that is even more pronounced in outdoor environment, where the amount of diffused light over direct irradiation can be estimated up to 17 %, as shown in Fig. 8. Moreover, here, the contribution of the bifacial Si HJT cell, play a role, being part of the sunlight transmitted from the rear of the spine to the back of the Si Cell. This extra source of light, and the contribution of the back side of the Si HJT cell, are not taken into consideration by the ideal model, explaining η^{EO} value above 100 %. As above noted, the η^{EO} increase, strong for the Si cell but negligible for the GaAs cell is consistent with spine transmittance. In conclusion, the very large η^{EO} increase for the Si cell in outdoor compared to indoor is likely due to the ability of the spines for the case of a white cover to collect more diffused sunlight, that is not present or almost null in the case of the indoor tests with the solar simulator.

3.3. Summary and conclusions

This study reports on the performances of a 4T solar cell system that uses spectral splitting and waveguiding low gain non optical asymmetrical concentrator to improve photovoltaic efficiency. The system is comprised of a commercial GaAs PV cell and a bifacial Si HJT cell, a DM and a custom made WDP. Spectral characterization of the optical components of the 4T system was performed, including transmittance and reflectance measurements of the DM, WDP, and the spine used to hold the overall system, as well as external quantum efficiency (EQE) analysis of the GaAs and Si HJT PV cells. The DM effectively reflected shorter wavelengths (from 400 nm to 790 nm) towards the GaAs PV cell, while transmitting longer wavelengths (beyond 805 nm) to the Si HJT PV cell, thereby optimizing the spectral response of each sub-cell.

The 4T system was tested in both indoor and outdoor environments to evaluate the impact of the incident angle of the source of light and of the colour of covers (white and black) applied to the spine on the measured photocurrent values and PV performance. Indoor experiments, by considering a Figure of Merit (FOM) analysis, revealed that the white cover performed noticeably better than the black cover at incidence angles for incoming light between 10° and 60°. This improvement is attributed to the ability of the spine in the case of a white cover to enhance light trapping in the system. Comparison of ideal and measured short-circuit current (I_{SC}) values further reinforced these findings, offering a deeper understanding of the optical coupling efficiency in different conditions. Outdoor experiments, under natural sunlight, confirmed the indoor results. The white cover configuration yielded much higher optical collection efficiencies for both the GaAs and Si HJT PV cells. Specifically, at a 20° incident angle (α_{noon}), the GaAs cell reached an impressive 90 % optical collection efficiency with the white cover, compared to 68 % with the black cover. Similarly, the Si HJT PV cell's optical collection efficiency at 10°, reached 115 % with the white cover, in comparison with the 49 % achieved with the black cover. These results definitively underscore the crucial role of diffused light in enhancing the performance of the white-covered system, particularly under in field conditions. These conclusions are valid for a small size 4T

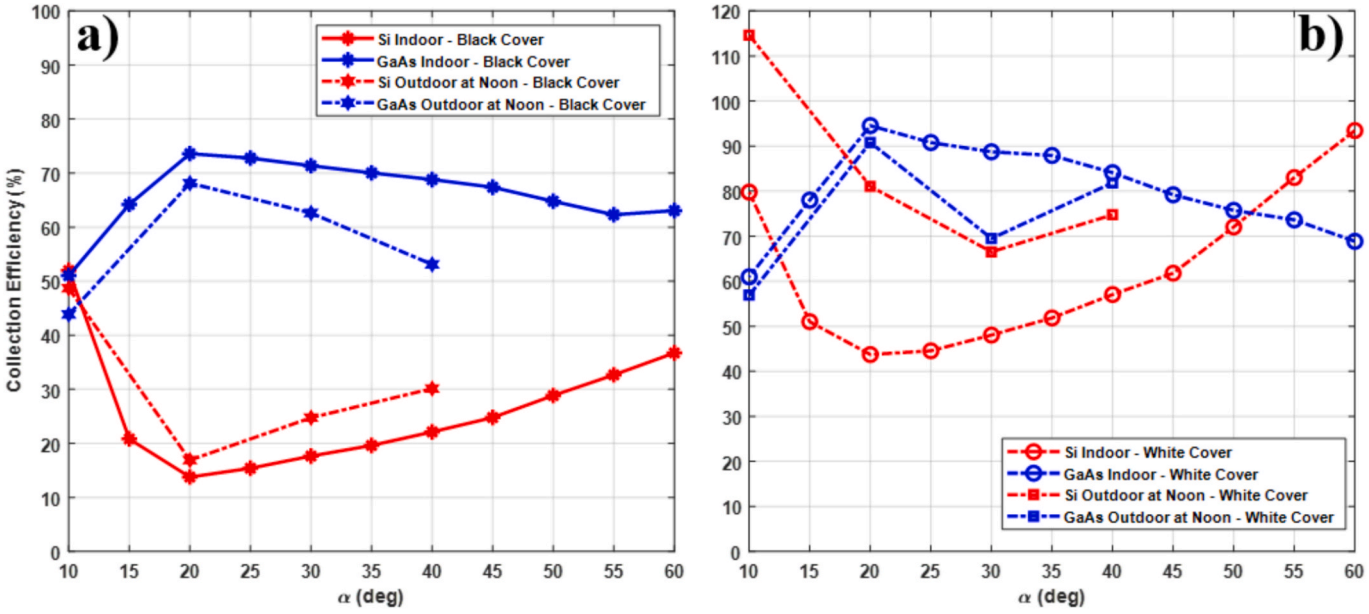

Fig. 12. Comparison of indoor and outdoor (at noon) efficiency at different α angles for the Si HJT and GaAs PV cells for the a) white and b) black cover cases.

PV system like the one presented, but need yet to be assessed for a large-scale system.

Furthermore, the study revealed the angular dependence of the optical collection efficiency for both cell types, emphasizing the importance of system orientation and tracking for maximizing energy generation in practical applications. While the FOM generally decreased with increasing incident angle, the use of a white cover reduced this effect, maintaining higher performance across the entire range of tested angles. As a perspective, a complementary dichroic mirror coupled to the VIS solar cell and a suitable installation height of the system in order to exploit the albedo collection at the rear face of a Silicon bifacial cell may further increase the system efficiency. Other measures, such as mounting the GaAs cell directly in contact with the WDP, using an index-matching liquid at all interfaces to prevent any air gap, and improving the short-wavelength transmittance by engineering the UV-stabilizers from a molecular level to find the best trade-off between UV-shielding and transparency, can all contribute to further improving system performance.

CRediT authorship contribution statement

Mehdi Ahmadi: Writing – review & editing, Writing – original draft, Validation, Software, Methodology, Formal analysis, Data curation, Conceptualization. **Roberto Pagano:** Writing – review & editing, Validation, Software, Data curation, Conceptualization. **Fabio Matera:** Investigation, Formal analysis. **Matteo Bonomo:** Writing – review & editing, Investigation, Conceptualization. **Simone Galliano:** Writing – review & editing, Investigation. **Iacopo Benesperi:** Investigation. **Claudia Barolo:** Writing – review & editing, Investigation. **Daniela Fontani:** Writing – review & editing, Methodology, Investigation. **Floriana Morabito:** Writing – review & editing, Investigation. **Andrea Farina:** Writing – review & editing, Investigation. **Silvia Maria Pietralunga:** Writing – review & editing, Methodology, Investigation, Funding acquisition, Conceptualization. **Salvatore Antonino Lombardo:** Writing – review & editing, Validation, Supervision, Software, Resources, Project administration, Methodology, Investigation, Funding acquisition, Formal analysis, Data curation, Conceptualization.

Declaration of competing interest

The authors declare that they have no known competing financial interests or personal relationships that could have appeared to influence the work reported in this paper.

Acknowledgements

M.A, R.P, F. M., A. F., D. F., S, M. P, and S. A. L gratefully acknowledge funding support from the PON Ricerca e Innovazione 2014-2020 Italian project ARS01_00519 BEST-4U. M.A, R.P, F. M., and S. A. L also acknowledge the IPHOQS Infrastructure "Integrated Infrastructure Initiative in Photonic and Quantum Sciences" (IR0000016) and the Research Infrastructure "Beyond-Nano" co-funded by Regione Sicilia (D.D.G. 2929/5S) and by Italian Ministry of University and Research (Decree 2510/2019). They also thank the invaluable graphic and editing help received from Michel Piliougine Rocha and Bahareh Sadat Jalilian. M.B., S.G., I.B. and C.B. acknowledge support from the project CH4.0 under the MUR (Italy) program "Dipartimenti di Eccellenza 2023–2027" (CUP: D13C22003520001). I.B. acknowledges support from the PNA4Energy project, funded under the MUR (Italy) program "PNNR M4C2 Initiative 1.2: Young Researcher - Seal of Excellence" (CUP: D18H22001950007), and thanks ICxT at the University of Turin for providing the 3D printer used to fabricate the wedge supports. S.G. acknowledges the project NODES which has received fundings from the MUR (Italy) - M4C2 1.5 of PNRR with grant agreement no. ECS00000036. M.B., S.G., I.B. and C.B. are also indebted with Demak Polymers s.r.l. for providing the precursors for the formulation of the dieletric wedge and for fruitful discussion.

S. M. P. and A. F. are authors of the international patent WO2024/003653 A1, published the 04/01/2024, having the title "Optical concentrator for four-terminal bifacial photovoltaic module".

Appendix A. Supplementary data

Supplementary data to this article can be found online at https://doi.org/10.1016/j.solener.2025.113934.

References

[1] International Energy Agency (IEA). *Net Zero by 2050: A Roadmap for the Global Energy Sector*. Paris (2023). https://www.iea.org/reports/net-zero-by-2050.
[2] IPCC, Climate Change 2021: The Physical Science Basis. Contribution of Working Group I to the Sixth Assessment Report of the Intergovernmental Panel on Climate Change. Cambridge University Press (2021). https://www.ipcc.ch/report/ar6/wg1/.
[3] W. Shockley, H.J. Queisser, Detailed balance limit of efficiency of p-n junction solar cells, J. Appl. Phys. 32 (3) (1961) 510–519, https://doi.org/10.1063/1.1736034.
[4] Luque, A., & Hegedus, S. (Eds.). *Handbook of Photovoltaic Science and Engineering*. John Wiley & Sons (2011). doi:10.1002/9780470974704.
[5] A. T. Raisa, S. N. Sakib, M. J. H., K. A. R., and A. Kowsar, *Advances in multijunction solar cells: An overview*. Solar Energy Advances, 5, 100105, (2025). doi:10.1016/j.seja.2025.100105.
[6] S. Li, et al., *Review of Multi-junction Solar Cell & Factors Impacting the Efficiency of Multi-junction Solar Cell*, Energy Sources Part A 45 (4) (2023) 12737–12758, https://doi.org/10.1080/15567036.2023.2275706.
[7] J. Li, et al., A brief review of high efficiency III-V solar cells for space application', Front. Phys. 8 (2021) 631925 https://doi.org/10.3389/fphy.2020.631925.
[8] I.M. Peters, et al., Practical limits of multijunction solar cells, Prog. Photovolt. Res. Appl. 31 (10) (2023) 1006–1015, https://doi.org/10.1002/pip.3705.
[9] A. Baiju, M. Yarema, *Status and challenges of multi-junction solar cell technology*, Front. Energy Res. 10 (2022) 971918, https://doi.org/10.3389/fenrg.2022.971918.
[10] S. Joseph Day, Senthilarasu, T.K. Mallick, Improving spectral modification for applications in solar cells: a review, Renew. Energy 132 (2019) 186–205, https://doi.org/10.1016/j.renene.2018.07.101.
[11] E. Raza, Z. Ahmad, Review on two-terminal and four-terminal crystalline-silicon/perovskite tandem solar cells; progress, challenges, and future perspectives, Energy Rep. 8 (2022) 5820–5851, https://doi.org/10.1016/j.egyr.2022.04.028.
[12] R. Corso, F. Matera, A. Scuto, & S. A. Lombardo. Outdoor Characterization of a Bifacial Four-Terminal GaAs/Si Mini-Module Under Different Albedo Conditions. In *2023 IEEE 50th Photovoltaic Specialists Conference (PVSC)* (pp. 1–3). San Juan, PR, USA, (2023). doi: 10.1109/PVSC48320.2023.10359731.
[13] Roberto Corso, Marco Leonardi, Rachela G. Milazzo, Andrea Scuto, Stefania M. S. Privitera, Marina Foti, Cosimo Gerardi, & Salvatore A. Lombardo. Evaluation of Voltage-Matched 2T Multi-Junction Modules Based on Monte Carlo Ray Tracing. *Energies, 16*, 4292, (2023). doi:10.3390/en16114292.
[14] A. Scuto, R. Corso, M. Leonardi, R.G. Milazzo, S.M.S. Privitera, C. Colletti, M. Foti, F. Bizzarri, C. Gerardi, S.A. Lombardo, Outdoor performance of GaAs/bifacial Si heterojunction four-terminal system using optical spectrum splitting, Sol. Energy 241 (2022) 483–491, https://doi.org/10.1016/j.solener.2022.06.032.
[15] A. Scuto, R. Corso, M. Leonardi, R.G. Milazzo, S.M.S. Privitera, C. Colletti, M. Foti, F. Bizzarri, C. Gerardi, S.A. Lombardo, Data on the design optimization, indoor characterization, and outdoor testing of GaAs/Bifacial Si heterojunction four-terminal photovoltaic systems, Data Brief 45 (2022) 108609, https://doi.org/10.1016/j.dib.2022.108609.
[16] R. Corso, M. Leonardi, A. Scuto, & S. A. Lombardo. Monte Carlo evaluation of multijunction solar systems in tandem and 4-terminal configurations. In *2022 IEEE 49th Photovoltaics Specialists Conference (PVSC)* (pp. 0551–0553). Philadelphia, PA, USA, (2022). doi: 10.1109/PVSC48317.2022.9938841.
[17] A.G. Imenes, D.R. Mills, Spectral beam splitting technology for increased conversion efficiency in solar concentrating systems: a review, Sol. Energy Mater. Sol. Cells 84 (1–4) (2004) 19–69, https://doi.org/10.1016/j.solmat.2004.01.038.
[18] A. Mojiri, R. Taylor, E. Thomsen, G. Rosengarten, Spectral beam splitting for efficient conversion of solar energy—A review, Renew. Sustain. Energy Rev. 28 (2013) 654–663, https://doi.org/10.1016/j.rser.2013.08.026.
[19] Kei Ito, Kazuteru Nonomura, Ryota Kan, Keishi Tada, Ching Chang Lin, Takumi Kinoshita, Takeru Bessho, Satoshi Uchida, & Hiroshi Segawa. Spectral Splitting Solar Cells Consisting of a Mesoscopic Wide-Bandgap Perovskite Solar Cell and an Inverted Narrow-Bandgap Perovskite Solar Cell. *ACS Omega, 9*, 3028–3034, (2024). doi:10.1021/acsomega.3c09654.
[20] M.B. Yücel, A. Cicek, B. Ulug, Polarization-independent beam splitting by a photonic crystal right prism, Appl. Phys. B 113 (2013) 107–114, https://doi.org/10.1007/s00340-013-5445-y.
[21] A. Pujari, T. Thomas, Aluminum nanoparticles alloyed with other earth-abundant plasmonic metals for light trapping in thin-film a-Si solar cells, Sustain. Mater. Technol. 28 (2021) e00250, https://doi.org/10.1016/j.susmat.2021.e00250.

[22] K. Araki, H. Tawa, H. Saiki, Y. Ota, K. Nishioka, M. Yamaguchi, The Outdoor Field Test and Energy Yield Model of the Four-Terminal on Si Tandem PV Module, Appl. Sci. 10 (7) (2020) 2529, https://doi.org/10.3390/app10072529.
[23] Hugo Sánchez, Carlos Meza, Sebastian Dittmann, & Ralph Gottschalg. The effect of clearance height, albedo, tilt and azimuth angle in bifacial PV energy estimation using different existing algorithms. In *Proceedings of the III Ibero-American Conference on Smart Cities (ICSC-2020),* (2020). Available at: https://www.researchgate.net/publication/346039220.
[24] R. Kopecek, J. Libal, Bifacial photovoltaics 2021: status, opportunities and challenges, Energies 14 (8) (2021) 2076, https://doi.org/10.3390/en14082076.
[25] C. Stanley, A. Mojiri, G. Rosengarten, Spectral light management for solar energy conversion systems, Nanophotonics 5 (1) (2016) 161–179, https://doi.org/10.1515/nanoph-2016-0035.
[26] M. Yamaguchi, F. Dimroth, J.F. Geisz, N.J. Ekins-Daukes, Multi-junction solar cells paving the way for super high-efficiency, J. Appl. Phys. 129 (24) (2021) 240901, https://doi.org/10.1063/5.0048653.
[27] Andrea Farina, Alice Carlotto, Stefano Varas, Alessandro Chiasera and Silvia Maria Pietralunga. An asymmetric low concentrator and spectral splitting approach to bifacial four-terminal photovoltaic modules. *Progress in Photovoltaics: Research and Applications, 31*, 1299–1314, (2023). doi:10.1002/pip.3644.
[28] L.V. Wang, Wu. Hsin-I, Biomedical Optics: Principles and Imaging, John Wiley & Sons, 2007.
[29] *Rera Solutions GaAs solar cell - Available at:* https://www.rerasolutions.com/product/gaas-reference-cell/. *Last accessed on 10/03/2025.*
[30] *SUN Tecnologia Core-H^{O} - Available at:* https://www.sun.com/it/prodotti. *Last accessed on 07/05/2025.*
[31] *Thorlabs dichroic mirror - Available at:* https://www.thorlabs.de/thorproduct.cfm?partnumber=DMLP805R. *(last seen 12 March 2025).*
[32] F. De Rossi, et al., *Thermosetting polyurethane-based encapsulation of flexible perovskite solar cells: a step forward in devices stabilization in highly damp environment*, Mater. Today Energy 49 (2025) 101850, https://doi.org/10.1016/j.mtener.2025.101850.
[33] Weather Underground - Available at: https://www.timeanddate.com/astronomy/italy/catania. (last seen 12 March 2025)..
[34] Air Mass 1.5 Spectra, NREL, url: https://www.nrel.gov/grid/solar-resource/spectra-am1.5.html (last seen 12 March 2025).
[35] Bacon, Amanda, Benjamin Harris, and Josh Klein. "Dichroic Filter Characterizations." arXiv preprint arXiv:2505.10702 (2025).
[36] F. De Rossi, D. Gallo, L. Bonandini, G. Koch, A. Menozzi, M. Bonomo, et al., Thermosetting polyurethane-based encapsulation of flexible perovskite solar cells: a step forward in devices stabilization in highly damp environment, Mater. Today Energy 49 (2025) 101850.